INSTITUTE OF PHYSICS PUBLISHING JOURNAL OF PHYSICS B: ATOMIC, MOLECULAR AND OPTICAL PHYSICS

J. Phys. B: At. Mol. Opt. Phys. **39** (2006) 1045–1053 doi:10.1088/0953-4075/39/5/004

A geometrical optics model for electron-molecule collisions

L G Ferreira[1], A R Lopes[1], M A P Lima[1] and M H F Bettega[2]

[1] Instituto de Física 'Gleb Wataghin', Universidade Estadual de Campinas, Caixa Postal 6165, 13083-970, Campinas, São Paulo, Brazil
[2] Departamento de Física, Universidade Federal do Paraná, Caixa Postal 19044, 81531-990, Curitiba, Paraná, Brazil

E-mail: luiz@gf1901.net

Received 25 November 2005, in final form 22 December 2005
Published 6 February 2006
Online at stacks.iop.org/JPhysB/39/1045

Abstract

We report the extension of a model, based on geometrical optics, that was developed to explain similarities found in the cross sections of electron collisions with small hydrocarbons. Here we discuss the modifications made in the model and apply it to electron-collisions with molecules containing other atoms besides carbon and hydrogen. We then apply the model to predict the cross sections for the larger molecules C_6H_6, C_8H_8, C_{60} and C_6F_6, and find that, even in this case, the model is useful for a first estimate of the theoretically calculated and experimental elastic cross sections.

(Some figures in this article are in colour only in the electronic version)

1. Introduction

In the past few years, several experimental studies concerning electron-collisions with hydrocarbons [1–5] motivated our group to investigate the so-called *isomer effect* [6–8], which is related to the differences in the cross sections of an isomeric group. The *isomer effect* allows one to distinguish between different isomers by their cross sections.

In calculating the electron elastic cross section of hydrocarbon isomers [8], we were surprised to verify that, for energies between 10 eV and 40 eV, the cross sections differed by a factor that could be calculated with a simple model burrowed from geometrical optics. The result was surprising because the range of energies implies electron wavelengths with the same order of the interatomic distances. Therefore, one would expect interference between the many atoms, which lies in the domain of the wave optics. Since the model worked very well for hydrocarbons, we decided to extend it to other atoms. This paper presents the details of the extension of the model for molecules containing other atomic species than carbon and hydrogen.

The outline of this paper is as follows. In the following section we discuss in details the model and its extension. In section 3, we present our results and discussions. We then end the paper with a brief summary.

2. Theory

In [8] we were surprised with the similarities seen in the hydrocarbon cross sections in two distinct situations: (1) through the comparison of hydrocarbons with different number of hydrogens, or different geometries, but the same number of carbons, one may conclude that the hydrogen atoms do not matter for electron scattering and that differences in geometry have a very small effect; (2) through the comparison of hydrocarbons with different numbers of carbons, one may note that their cross sections seem to differ only by a scale factor that depends on the energy of electron beam.

The model we proposed in [8] to explain the similarities discussed above is as follows. We considered spheres of radii R centred at the molecular carbon sites. We distinguished three carbon types: those with four neighbours ($C^{(4)}$), those with three neighbours ($C^{(3)}$) and those with two neighbours ($C^{(2)}$). Of course the less neighbours a carbon atom has the more π binding orbitals it has. Thus, it was natural to assume that the sphere radii depend on the number of neighbours. Later we found the distinction not important. On this molecule of spheres we impinge light rays randomly oriented and calculate the area of the shadow on a screen behind the molecule. The calculation of the shadow area is made with the Monte Carlo technique because of the confusing intersections of the many sphere projections on the screen. Thus, for a given randomly oriented ray hitting at random point of a sphere, we check whether the ray also hit another sphere, in which case the ray is eliminated from the count if it was reckoned previously. For the hydrocarbons that we calculate we used up to 83 million randomly oriented rays to calculate the average shadow (geometric cross section). If the radius tends to zero naturally the ratio tends to the number of carbons. If the radius tends to infinity, the distances between centres become relatively negligible and the shadow tends to that of a single sphere. In this case, the ratio tends to 1.

For a generic hydrocarbon, the calculation of the average shadow only required knowledge of the carbon atomic positions and the sphere radii $R^{(4)}$, $R^{(3)}$, $R^{(2)}$, corresponding to the carbons with four, three and two neighbours, respectively (though H did not contribute to the cross section or shadow, they were counted as neighbours of carbons.). The radii were assumed to depend on the incident electron energy. We determined the radii as follows. First we equated the ratios

$$\frac{\sigma(E, \mathrm{CH_4}, \mathrm{SMC})}{\sigma(R^{(4)}, \mathrm{CH_4}, \mathrm{shadow})} = \frac{\sigma(E, \mathrm{C_2H_6}, \mathrm{SMC})}{\sigma(R^{(4)}, \mathrm{C_2H_6}, \mathrm{shadow})}$$

of the SMC-calculated cross section and shadow for the molecules CH_4 and C_2H_6, both having carbons with four neighbours, to determine $R^{(4)}$ as function of energy. Then we used the equations

$$\frac{\sigma(E, \mathrm{CH_4}, \mathrm{SMC})}{\sigma(R^{(4)}, \mathrm{CH_4}, \mathrm{shadow})} = \frac{\sigma(E, \mathrm{C_2H_4}, \mathrm{SMC})}{\sigma(R^{(3)}, \mathrm{C_2H_4}, \mathrm{shadow})} = \frac{\sigma(E, \mathrm{C_2H_2}, \mathrm{SMC})}{\sigma(R^{(2)}, \mathrm{C_2H_2}, \mathrm{shadow})}$$

to determine $R^{(3)}$ and $R^{(2)}$.

Having the radii, we were able to compute the shadow cross section for several hydrocarbons and noted that the dispersion was about $\simeq$5% and that the ratio was around 2.0.

After the success of the model for the hydrocarbons, the next natural step was to extend it to other atoms and molecules. To deal with many atomic species we had to slightly modify the model. Now the atomic radii, which depends on the incident electron energy, are calculated

by minimizing the following expression:

$$\sum_m \left[\frac{\sigma(E, m, \text{SMC})}{\sigma(\{R\}, m, \text{shadow})} - X \right]^2 = \text{minimum}, \tag{1}$$

where $\sigma(E, m, \text{SMC})$ is the cross section computed by the Schwinger multichannel method (SMC) [9] with pseudopotentials [10] and $\sigma(\{R\}, m, \text{shadow})$ is the geometrical shadow area. Here m are molecules of a set and $\{R\}$ is a set of atomic radii. We considered a set of 35 molecules and nine atomic species (a set of nine radii). We verified that the minimum in equation (1) depends a little on the chosen value of X. Thus, we set

$$X = 2$$

because in [8], when X was optimized, we verified that its value was near 2.

There is a subtler reason for the choice $X = 2$. For the scattering from a hard sphere, the s-wave cross section is well known to be $4\pi R^2$, namely four times the area of the geometrical shadow projection. The s-wave scattering is the main scattering when the energy is low. As the energy increases, the cross section tends to $2\pi R^2$ corresponding to our choice of $X = 2$ [15, 16]. Of course, the molecules that we calculated are not hard spheres. Hopefully, the energies we are working with are large enough to overcome some centrifugal barriers, and small enough so that the atoms present themselves as hard spheres to the incident electron.

It is interesting to question whether the shadow model has any justification in a hard-core physics. Being a model derived from optics whose analogue in the electron scattering problem is the Born approximation, we calculated the electron-scattering Born cross section for several model potentials M of molecules M_4 (a regular tetrahedron), M_3 (a triangle), M_2 (a pair) and M (an atom). A typical result is presented in figure 1, about which we make the following comments:

- The model potential presented is a smooth combination of Gaussians. This behaviour is what one expects due to the orthogonalization of the scattering orbital to the valence and core orbitals.
- The shadow model will work as long as

  $$\frac{1}{n}\sigma(M_n) \leqslant \frac{1}{p}\sigma(M_p) \quad \text{for} \qquad n > p$$

  and the atoms of M_p occupying sites of M_n that is, an atom may hide others behind. In figure 1 , this behaviour is observed in the energy band from 1.0 to 5.0. Outside this band the shadow model is clearly inadequate because one obtains 'negative' shadows.
- For the energies in the range where the shadow model works, we expected scattering cross sections decreasing with energy. In the Born case, figure 1 shows this to be only partially true.

Thus, the Born model points to the possibility of the shadow model working for special potentials and energy ranges. But the Born approximation is a poor approximation (failure of the optical theorem, for instance), so that the true justification of the shadow model remains its compatibility with the precise calculations that match experiment very well.

Equation (1) was used in nine minimizations. The first considered only the molecule H_2 from which we obtained the radius of the H sphere. Next, we used the equation for the molecules SiH_4, GeH_4, SnH_4, HF to obtain the radii of Si, Ge, Sn, F. In each minimization, we had only one molecule and one radius parameter. Next, we used the equation for the molecules CH_4, C_2H_6 and C_2H_4 to obtain the radius of C. In this case we dealt with three molecules and just one radius parameter. Observe that, unlike [8], here we are using a single radius for C, independently of the number of neighbours. In [8] we verified that the number of neighbours

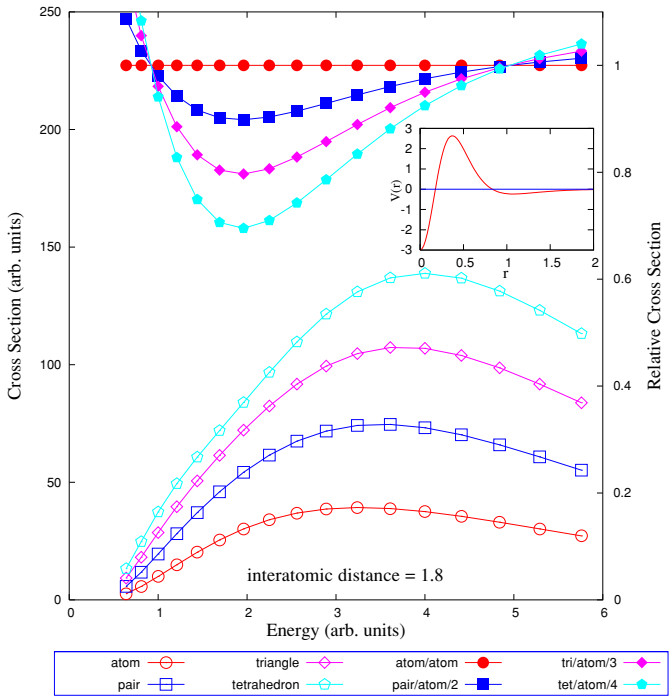

Figure 1. Born cross sections for the model potential of the inset, arranged as an atom, an atom pair, a triangle and a tetrahedron. The interatomic distances are equal to 1.8 in all cases. Observe that the cross sections have a decaying behaviour only for energies larger than 4.0. The ratios of the cross sections to that of a single atom, divided by the number of atoms in each arrangement, is shown in the top part of the figure. The ratios are smaller than 1.0 for energies between 1.0 and 5.0. For the shadow model to work, it is absolutely necessary that the ratio be smaller than 1.0, meaning that an atom is hiding another atom behind.

was a minor effect determining the radius of the sphere. Next, we considered nine molecules containing Cl and atoms whose radii were already determined, thus again a minimization with just one parameter, the radius of Cl. Next came the case of nine molecules of Br to determine the radius of this atom, and finally the case of nine molecules of I. Therefore, in all minimizations, we dealt with a single parameter.

Before discussing the results we must say a word on how to calculate the shadow area of the assembly of atomic spheres, a problem which is not completely trivial. Figure 2 shows the shadows of four atomic spheres. To calculate the molecular shadow, the overlap regions must be counted just once. Because the boundaries of the overlap regions may become complicate we proceeded as follows. First, we order the atoms arbitrarily. Then we start shooting light rays on the atoms i randomly distributed in the range $\left[0, R_i^2\right]$ of r^2 values and in the range $[0, 2\pi]$ of ϕ values. Letting $N_{r^2} N_\phi$ be the number of shots, each one gives a contribution $\pi R_i^2 \big/ (N_{r^2} N_\phi)$ to the molecular shadow, except if it also hits a previous atomic sphere, in which case the shot does not contribute to the shadow area. Aside from shooting randomly on the atomic discs, the directions of the shots were also chosen randomly. Therefore, the total number of shots was

$$\begin{aligned}\text{Number of shots} &= (\text{Number of directions}) \times (\text{Number of } r^2) \\ &\quad \times (\text{Number of } \phi) \times (\text{Number of atoms}) \\ &= 35^2 \times 35 \times 35N,\end{aligned}$$

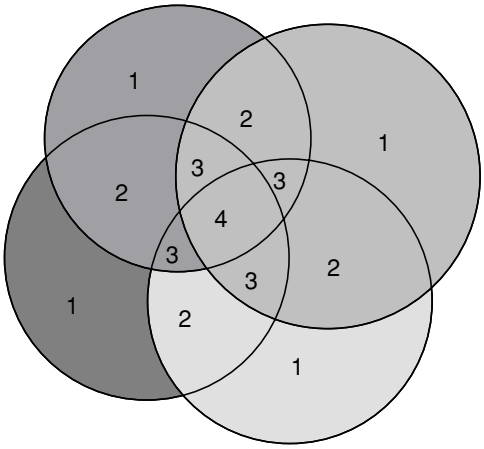

Figure 2. Figure to show many intersections of the atomic shadows composing the molecular shadow. The area of the intersections must be counted only once.

Table 1. Shadow radii (a_0) as functions of energy (eV).

Energy	H	C	Si	Ge	Sn	F	Cl	Br	I
15	1.539	3.372	4.082	3.907	3.629	2.222	3.487	3.598	3.805
20	1.304	3.089	3.576	3.283	2.706	2.197	3.283	3.317	3.318
25	1.135	2.811	3.251	2.777	2.049	2.261	3.066	3.009	2.802
30	0.993	2.533	2.997	2.402	1.726	2.195	2.823	2.679	2.352
35	0.888	2.304	2.746	2.082	1.475	2.102	2.602	2.389	1.987
40	0.802	2.111	2.491	1.850	1.288	1.998	2.399	2.120	1.679

where the integer 35 was chosen so that the statistical errors were in the order of 0.1% or less. Thus, our calculation of the shadow, because of the complicate domains of integration as shown by the many intersections in figure 2, follows the Monte Carlo method as described in [17, 18]. Our choice of a statistical error in the order of 0.1% was of course an overkill, yet the calculations were very fast in a desk computer. In the appendix we show in detail how to calculate the shadow area.

3. Results

Figure 3 presents the results for the ratios of the SMC cross section divided by the shadow area (equation (1)). The line crossing the data points corresponds to the nominal value of $X = 2$. The molecules are numbered according to the order of the minimization. One observes that, aside from a dispersion that increases with energy, many molecules do not deviate much from the nominal ratio $X = 2$. The atomic radii are tabulated in table 1 and plotted in figure 4. They are in no way similar to radii of standard tables (atomic or covalent) [14], for instance Si is larger than Sn. Their behaviour as a function of energy is represented in figure 4. The radii decrease with energy, or as the wavelength becomes smaller. That can be understood in the following terms. As the wavelength becomes smaller, different atomic regions scatter out of phase so that the net result is smaller.

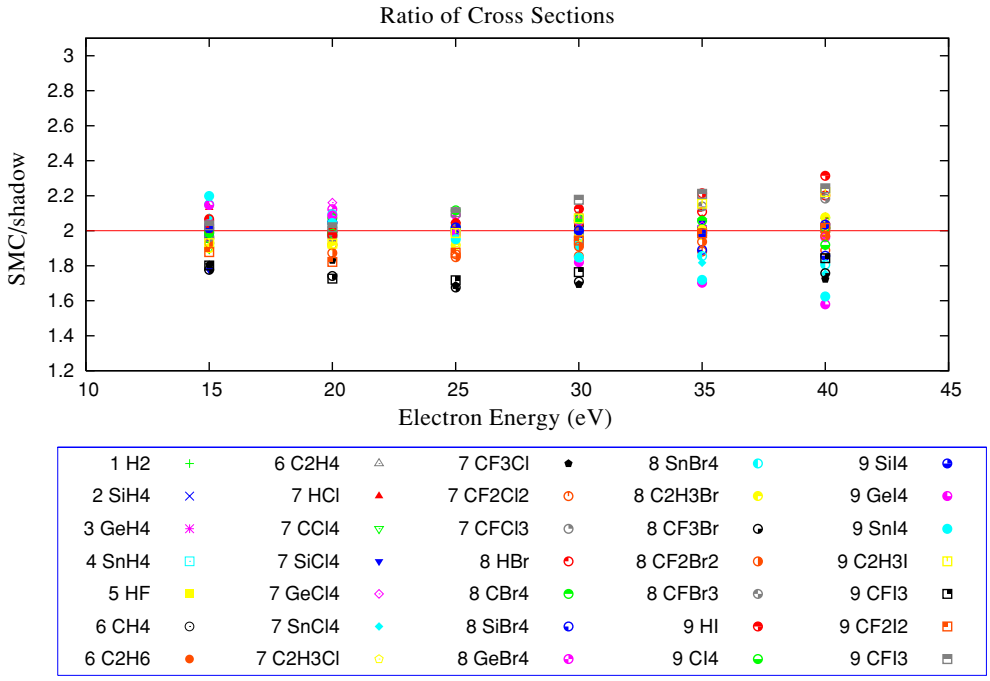

Figure 3. Ratio of cross sections (SMC/shadow area) of electron-molecule elastic collisions against electron energy (eV). The molecules are ordered as they were used to determine the radii: H, Si, Ge, Sn, F, C, Cl, Br, I.

The result presented in figure 3 is somewhat surprising because, at a typical energy in the range, the wavelength is comparable to the molecular sizes

$$20\ \text{eV} \longrightarrow \lambda \simeq 5.2\ \text{au}.$$

One notices that, as the energy increases to 40 eV, the shadow model becomes poorer, as it is evidenced by the larger spread of the data points. If the molecule is large enough, one may expect that its different atoms will scatter with different phases, even destructively. Apparently the ratio $size/\lambda$ determines the quality of the model. If the ratio is large one may expect a worse fit to calculated or measured cross sections, and possibly an exaggerated estimate thereof. Table 2 shows four instances in which the shadow model is used to predict the results of cross section calculations and experiment. Two comments are in order. First, the molecules of table 2 are larger than the molecules used to calculate the shadow radii. Second, the measured cross sections are elastic, not total. It is to be observed in the table that, in general, the shadow model seems to give results bigger than either calculation or experiment, but yet with quality for a first and simple estimate of cross sections.

Acknowledgments

ARL acknowledges scholarship from Brazilian agency Fundação de Amparo à Pesquisa do Estado de São Paulo (FAPESP). MHFB, MAPL and LGF acknowledge support from Brazilian agency Conselho Nacional de Desenvolvimento Científico e Tecnológico (CNPq). MHFB also acknowledges support from the Paraná state agency Fundação Araucária, from FINEP (under

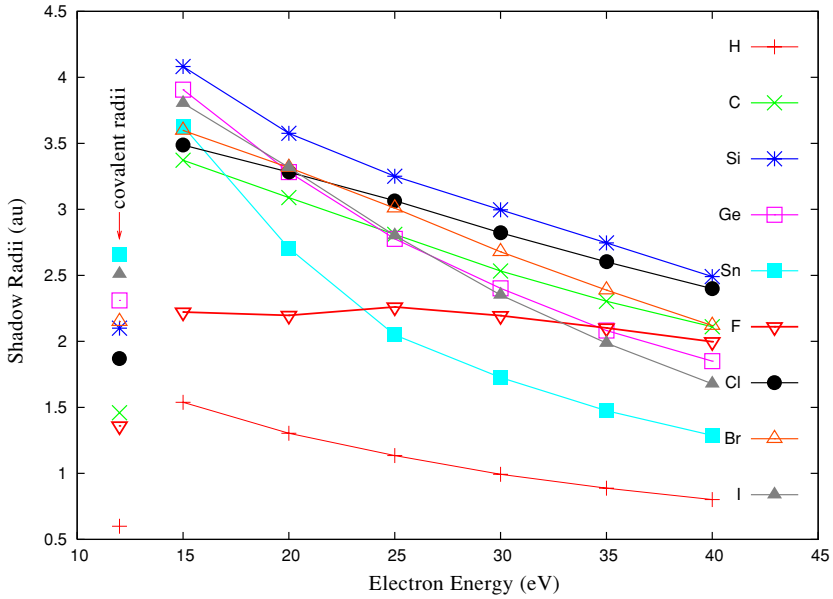

Figure 4. Shadow radii as functions of energy. The radii were determined according to equation (1) with $X = 2$ in the following order: H, Si, Ge, Sn, F, C, Cl, Br, I. In each determination the molecules used were those numbered in figure 3. In the left-hand side, we mark the covalent radii for comparison [14].

Table 2. Elastic cross section predictions compared to calculated and experimental results (a_0^2).

	Benzene (C_6H_6)			Cubane (C_8H_8)		Fullerene (C_{60})		Hexafluorobenzene C_6F_6	
Energy (eV)	Predictions	Calculated [13]	Experimental [19]	Predictions	Calculated [11]	Predictions[a]	Calculated [12]	Predictions	Experimental [19]
15	173	160	$121 \pm 25\%$	190	179	601	490	203	$184 \pm 25\%$
20	154	140	$119 \pm 25\%$	171	154	568	490	197	$171 \pm 25\%$
25	139	130		153	147	533	433	197	
30	123	115	$111 \pm 25\%$	138		500	433	187	$117 \pm 25\%$
35	112	107		126		473		177	
40	102	99	$96 \pm 25\%$	116		451		170	

[a] We used the truncated icosahedron with 6–6 and 6–5 bond lengths following Hawkins *et al* [20].

project CT-Infra 1) and from Professor Carlos M de Carvalho for computational support at DF–UFPR. Part of these calculations were carried out at CENAPAD-SP.

Appendix. The calculation of the molecular shadow

- First, order the atoms from $i = 1$ to N_a. Each atom is a sphere of radius R_i centred at $\vec{r}_i$. The order is arbitrary.
- The direction of the shots must be random because we are interested in the cross section, not in the differential cross section. Thus, we choose $N_{\cos\Theta} N_\Phi$ random directions by randomly picking a $\cos\Theta$ in the range $[-1, 1]$ and a Φ in the range $[0, 2\pi]$. Therefore, the direction of the shots are along the unit vectors

$$\hat{u}_3 = \sin\Theta\cos\Phi\hat{e}_1 + \sin\Theta\sin\Phi\hat{e}_2 + \cos\Theta\hat{e}_3$$

which, together with

$$\begin{aligned}\hat{u}_1 &= \cos\Theta\cos\Phi\hat{e}_1 + \cos\Theta\sin\Phi\hat{e}_2 - \sin\Theta\hat{e}_3\\ \hat{u}_2 &= -\sin\Phi\hat{e}_1 + \cos\Phi\hat{e}_2\end{aligned} \tag{A.1}$$

forms a triorthonormal vector system. The unit vector $\hat{e}_1$ is randomly chosen among $\hat{x}$, $\hat{y}$ and $\hat{z}$, and so is $\hat{e}_2$ (excluding the vector chosen for $\hat{e}_1$), while $\hat{e}_3 = \hat{e}_1 \times \hat{e}_2$. In this way we avoid the asymmetry between x, y and z in the spherical coordinate system.

- For a given direction, we begin shooting the atoms with light rays to determine the shadow area. Suppose we have already the shadow area of the set of the first $(I-1)$ atoms. For the Ith atom we are going to shoot $N_\phi N_{r^2}$ light rays on the disc projection of the Ith sphere, where ϕ is chosen randomly in the range $[0, 2\pi]$ and r^2 chosen randomly in the range $\left[0, R_I^2\right]$.
- To each shot we assign an area equal to $\pi R_I^2 \big/ (N_\phi N_{r^2})$. Then we must check whether this shot also hits the disc projection of a previous sphere. If it does not hit the disc of any atom i from 1 to $(I-1)$, then we increment the molecular shadow area by $\pi R_I^2 \big/ (N_\phi N_{r^2})$.
- To verify that the shot does not hit a previous disc, we proceed as follows. The centre of the Ith sphere is at $\vec{r}_I$, therefore, the shot $[r^2, \phi]$ hits the screen behind the molecule at

$$\vec{\rho} = (\vec{r}_I \cdot \hat{u}_1 + r\cos\phi)\hat{u}_1 + (\vec{r}_I \cdot \hat{u}_2 + r\sin\phi)\hat{u}_2$$

The centre of a previous sphere i is at $\vec{r}_i$ and the distance between the projection of this centre and vector $\vec{\rho}$ must be greater than R_i.

$$(\vec{r}_I \cdot \hat{u}_1 + r\cos\phi - \vec{r}_i \cdot \hat{u}_1)^2 + (\vec{r}_I \cdot \hat{u}_2 + r\sin\phi - \vec{r}_i \cdot \hat{u}_2)^2 > R_i^2$$

$$\longrightarrow \text{ shot does not hit atom } i$$

- Randomly choose another pair $[r^2, \phi]$ and repeat till the number of pairs equal $N_{r^2} N_\phi$.
- Go to the next atom $I+1$, and to the next till one reaches the N_a atoms.
- Randomly choose another shot direction $[\cos\Theta, \Phi]$ and unit vectors $\hat{e}_1$ and $\hat{e}_2$ and repeat till the number of directions equal $N_\Theta N_\Phi$.
- Therefore, the total number of shots is $N_a N_\Theta N_\Phi N_{r^2} N_\phi$.

References

[1] Nakano Y, Hoshino M, Kitajima M, Tanaka H and Kimura M 2002 *Phys. Rev.* A **66** 032714
[2] Makochekanwa C, Kawate H, Sueoka O, Kimura M, Kitajima M, Hoshino M and Tanaka H 2003 *Chem. Phys. Lett.* **368** 82
[3] Szmytkowski Cz and Kwitnewski S 2002 *J. Phys. B: At. Mol. Opt. Phys.* **35** 3781
[4] Szmytkowski Cz and Kwitnewski S 2003 *J. Phys. B: At. Mol. Opt. Phys.* **36** 2129
[5] Szmytkowski Cz and Kwitnewski S 2002 *J. Phys. B: At. Mol. Opt. Phys.* **35** 2613
[6] Lopes A R and Bettega M H F 2003 *Phys. Rev.* A **67** 032711
[7] Lopes A R, Lima M A P, Ferreira L G and Bettega M H F 2004 *Phys. Rev.* A **69**
[8] Lopes A R, Bettega M H F, Lima M A P and Ferreira L G 2004 *J. Phys. B: At. Mol. Opt. Phys.* **37** 997
[9] Takatsuka K and McKoy V 1981 *Phys. Rev.* A **24** 2473
Takatsuka K and McKoy V 1984 *Phys. Rev.* A **30** 1734
[10] Bettega M H F, Ferreira L G and Lima M A P 1993 *Phys. Rev.* A **47** 1111
[11] Gianturco F A, Lucchese R R, Grandi A and Sana N 2004 *J. Chem. Phys.* **120** 4172
[12] Lucchese R R, Gianturco F A and Sana N 1999 *Chem. Phys. Lett.* **305** 413
Lucchese R R and Gianturco F A 1999 *J. Chem. Phys.* **111** 6769
Lucchese R R, Gianturco F A and Sana N 1999 *J. Phys. B: At. Mol. Opt. Phys.* **32** 2181
[13] Bettega M H F, Winstead C and McKoy V 2000 *J. Chem. Phys.* **112** 8806
[14] http://www.webelements.com
[15] Shankar R 1994 *Principles of Quantum Mechanics* 2nd edn (Dordrecht: Kluwer) p 554
[16] Sakurai J J 1995 *Modern Quantum Mechanics* revised edn (Reading, MA: Addison-Wesley) p 409

[17] Eric W and Weisstein E W "Monte Carlo Integration" MathWorld—A Wolfram Web Resource http://mathworld.wolfram.com/MonteCarloIntegration.html
[18] Demidovitch B and Maron I 1979 *'Eléments de Calcul Numérique* 2nd edn (Moscow: Mir) p 648 (French Transl.)
[19] Cho H, Gulley R J, Sunohara K, Kitajima M, Uhlmann L J, Tanaka H and Buckman S J 2001 *J. Phys. B: At. Mol. Opt. Phys.* **34** 1019–38
[20] Hawkins J M, Meyer A, Lewis T A, Loren S and Hollander F J 1991 *Science* **252** 312